Reliability Investigation on Numerical Analysis by Comparison with Experimental Result

**Satoshi Adachi [†], Keisuke Kawachi [††], Minoru Kaneko [†††],
Hirokazu Kato [††††], Shin-ichi Yoda [††††], and Kyoichi Kinoshita [†††††,†††††]**

[†]   Fundamental Technology Dept, Research Institute, Ishikawajima-Harima Heavy Industries
Co., Ltd., 1-15, Toyosu 3-chome, Koto-ku, Tokyo, 135-8732 Japan

[††]   Space Experiment System Development Department, Space Development Division,
Aero-Engine & Space Operations, Ishikawajima-Harima Heavy Industries Co., Ltd., 229,
Tonogaya, Mizuho-cho, Nishi-Tama-gun, Tokyo, 190-12, Japan

[†††]   Space Dept, Ishikawajima Jet Service Co., Ltd., 1-15, Toyosu 3-chome, Koto-ku, Tokyo,
135-8732 Japan

[††††]   Space Utilization Research Center, Office of Space Utilization Systems, National Space
Development Agency of Japan, 2-1-1, Sengen, Tsukuba-shi, Ibaraki, 305-8505 Japan

[†††††]   Wide-Bandgap Semiconductor Research Group, Physical Science Laboratory, NTT Basic
Research Laboratories, 3-1, Morinosato Wakamiya, Atsugi-shi, Kanagawa, 243-0198 Japan

In order to investigate conditions to grow semiconductor crystals with convex solid-liquid interface under microgravity, numerical calculations have been carried out. The calculation code is based on the boundary fitted coordinate (BFC) method. The current code has been improved so as to simultaneously solve nonsteady governing equations, such as an energy transport equation, a vorticity transport equation, a stream function equation, and an energy balance equation. By using this code, both interface location and interface shape change are traced for various gravity levels. In order to investigate reliability of the calculation, a ground-based experiment is carried out. From the comparison of these results, it is clarified that the numerically obtained initial interface shape well agrees with the experimentally obtained one. In order to obtain the trend of the shape change, the shape is fitted by a parabolic function and a proportional coefficient of the second order term is obtained. The trend of the experimental result is about twice as steep as that obtained by calculation. However, calculated temperature profiles well agree with experimentally measured temperatures.

1. Introduction

In a melt growth technique using a crucible such as the Bridgeman method, a shape of a solid-liquid interface should be convex toward the melt in order to grow a single crystal. Generally, a grain boundary macroscopically will grow perpendicularly to the interface. Therefore, if the interface shape is convex, nuclei appearing around the crucible wall will be caught by with the wall, and then will be eliminated before developing into a grain boundary.

On the earth, the convex shape can be achieved by optimizing growth conditions and by modifying a furnace suitable for the material.

However, in the microgravity experiments, it is difficult to optimize a furnace for one material due to a multipurpose furnace. Furthermore, limitations such as safety, power resources, weight and size make this optimization more difficult. Therefore, an interface shape is concave [1,2] in the past melt growth experiment under microgravity. Since only polycrystals or small single crystals can be obtained due to the concavity, the effectiveness of the microgravity experiments begins to be doubted.

In order to clear away such a doubt, it is required that a large single crystal enough to evaluate the characteristics must be obtained in

the micrographity experiment. For this purpose, it is one of the extreme priority subjects to make the interface shape convex under the microgravity. However, the timely and various improvement of the furnace for the microgravity experiment being similar to that on the earth is difficult as mentioned above. Thus, it is required improving performance of an ampoule and a cartridge to compensate the furnace performance [2, 3].

In order to get the suitable configuration of the ampoule and the cartridge for the convex shape, numerical analysis has been carried out. In order to obtain more precise results, the calculation code has been improved. The code of the current version can solve nonsteady simultaneous governing equations of energy transport, vorticity transport, stream function, and energy balance. Therefore, the code can trace the interface location and the shape change from moment to moment.

In this study, the performance of the present candidates of the flight ampoule and the flight cartridge is investigated by the numerical analysis. The reliability of the calculation result is also investigated by comparing with ground-based experimental results. To discuss the reliability, the tendency of the interface shape change in the calculation result is compared with the change in the experimental result. The temperature profiles are also compared.

In this paper, the mathematical model is described in the next section, then the calculation result, the experimental result on the ground, and discussion are described, and finally the results are summarized.

2. Mathematical Model

In this study, the boundary fitted coordinate (BFC) method [4-7], which is a kind of a finite difference method, is used. The BFC method solves the governing equations that are transformed from the physical space to the computational space. The BFC method has a feature of automatic grid generation. In this study, the method of the grid generation based on the Poisson equation is used. This method is well known as one of the methods of generating a smooth grid.

In this paper, it is assumed that the interface is determined by only the temperature, that is, the material is assumed to be the element or the binary compound. Thus the governing equations that have to be solved are the energy transport equation, the vorticity transport equation, the stream function equation, and the energy balance equation. In this study, the cylindrical coordinates are used by considering a typical flight sample shape. Therefore, the governing equations are described as follows;

$$\rho \, C_p \frac{\partial T}{\partial t}$$
$$+ \rho \, C_p \left(\frac{1}{r} \frac{\partial \psi}{\partial z} \frac{\partial T}{\partial r} - \frac{1}{r} \frac{\partial \psi}{\partial r} \frac{\partial T}{\partial z} \right) \quad , \quad (1)$$
$$= \kappa \left(\frac{\partial^2 T}{\partial r^2} + \frac{1}{r} \frac{\partial T}{\partial r} + \frac{\partial^2 T}{\partial z^2} \right)$$

$$\frac{\partial \omega}{\partial t} + \frac{1}{r} \frac{\partial \psi}{\partial z} \frac{\partial \omega}{\partial r} - \frac{1}{r} \frac{\partial \psi}{\partial r} \frac{\partial \omega}{\partial z}$$
$$- \frac{1}{r^2} \omega \frac{\partial \psi}{\partial z}$$
$$= \nu \left(\frac{\partial^2 \omega}{\partial r^2} + \frac{1}{r} \frac{\partial \omega}{\partial r} + \frac{\partial^2 \omega}{\partial z^2} - \frac{1}{r^2} \omega \right) \quad , \quad (2)$$
$$+ B \, g \frac{\partial T}{\partial r}$$

$$- r\omega = \frac{\partial^2 \psi}{\partial r^2} - \frac{1}{r} \frac{\partial \psi}{\partial r} + \frac{\partial^2 \psi}{\partial z^2} \quad , \text{and,} \quad (3)$$

$$L_{SL} \, \rho \, u \cdot \hat{n} = -\kappa_L \left(\frac{\partial T}{\partial n} \right)_L + \kappa_S \left(\frac{\partial T}{\partial n} \right)_S \quad , \quad (4)$$

where, ψ is the stream function, ω vorticity, T temperature, ρ density, C_p specific heat, κ thermal conductivity, ν kinetic viscosity, L_{SL} latent heat, B thermal volume expansion coefficient, g gravity, r radius, z length, t time, u moving velocity vector of the interface, $\hat{n}$ normal unit vector to the interface. Subscriptions of L and S indicate the liquid side and the solid side, respectively.

Here, before the physical coordinates are transformed to the computational coordinates, Equation (4) must be transformed to the scalar expression. In this transformation, it is assumed that the interface shape and its location can be

expressed by using any function f , that is,

$$z = f(r,t) \quad . \qquad (5)$$

By using eq. (5), the normal unit vector $\hat{n}$ can be described as

$$\hat{n} = \frac{1}{\sqrt{1+\left(\dfrac{\partial f}{\partial r}\right)^2}}\left(-\frac{\partial f}{\partial r},\, 1\right) \quad . \qquad (6)$$

This equation is substituted to the right side of eq. (4);

(Right Side)

$$\equiv -\kappa_L \left(\nabla T\right)_L \cdot \hat{n} + \kappa_S \left(\nabla T\right)_S \cdot \hat{n}$$

$$= \frac{1}{\sqrt{1+\left(\dfrac{\partial f}{\partial r}\right)^2}}\left\{-\kappa_L\left(\frac{\partial T}{\partial z}-\frac{\partial T}{\partial r}\frac{\partial f}{\partial r}\right)\right.$$

$$\left.+\kappa_S\left(\frac{\partial T}{\partial z}-\frac{\partial T}{\partial r}\frac{\partial f}{\partial r}\right)\right\} \qquad (7)$$

On the other hand, the left side of eq. (4) is represented as;

$$(\text{Left Side}) = \frac{L_{SL}\,\rho}{\sqrt{1+\left(\dfrac{\partial f}{\partial r}\right)^2}}\frac{\partial f}{\partial t} \quad . \qquad (8)$$

By combining eqs. (7) and (8), eq. (4) can be expressed as

$$L_{SL}\,\rho\frac{\partial f}{\partial t}=\left\{-\kappa_L\left(\frac{\partial T}{\partial z}-\frac{\partial T}{\partial r}\frac{\partial f}{\partial r}\right)_L\right.$$

$$\left.+\kappa_S\left(\frac{\partial T}{\partial z}-\frac{\partial T}{\partial r}\frac{\partial f}{\partial r}\right)_S\right\} \qquad (9)$$

The governing equations, eqs. (1) – (3) and (9), are transformed from the physical coordinates, r and z , to the computational coordinates, ξ and η . However, the transformation requires relationship between the physical space and the computational space. The relationship between minute elements in both spaces can be expressed as

$$\begin{pmatrix} d\xi \\ d\eta \end{pmatrix}=\begin{pmatrix} \xi_r & \xi_z \\ \eta_r & \eta_z \end{pmatrix}\begin{pmatrix} dr \\ dz \end{pmatrix} \quad , \text{and} \qquad (10)$$

$$\begin{pmatrix} dr \\ dz \end{pmatrix}=\begin{pmatrix} r_\xi & r_\eta \\ z_\xi & z_\eta \end{pmatrix}\begin{pmatrix} d\xi \\ d\eta \end{pmatrix} \quad . \qquad (11)$$

Subscriptions indicate the partial differentials. Equation (11) can be rewritten as

$$\begin{pmatrix} d\xi \\ d\eta \end{pmatrix}=\frac{1}{J}\begin{pmatrix} z_\eta & -r_\eta \\ -z_\xi & r_\xi \end{pmatrix}\begin{pmatrix} dr \\ dz \end{pmatrix} \quad , \qquad (12)$$

where J is Jacobian, $r_\xi z_\eta - r_\eta z_\xi$.
By comparing eq. (10) with eq. (12), the relationship is obtained as follows;

$$\xi_r = \frac{z_\eta}{J}, \quad \xi_z = -\frac{r_\eta}{J},$$

$$\eta_r = -\frac{z_\xi}{J}, \quad \eta_z = \frac{r_\xi}{J} \quad . \qquad (13)$$

The partial differentials by the component corresponding to the physical coordinates can be expressed by using eq. (13), that is,

$$\frac{\partial}{\partial r}=\frac{z_\eta}{J}\frac{\partial}{\partial\xi}-\frac{z_\xi}{J}\frac{\partial}{\partial\eta} \quad , \qquad (14)$$

$$\frac{\partial}{\partial z}=-\frac{r_\eta}{J}\frac{\partial}{\partial\xi}+\frac{r_\xi}{J}\frac{\partial}{\partial\eta} \quad , \qquad (15)$$

$$\frac{\partial^2}{\partial r^2}$$

$$=\frac{1}{J^2}\left(z_\eta^2\frac{\partial^2}{\partial\xi^2}\right.$$

$$\left.-2z_\xi z_\eta\frac{\partial^2}{\partial\xi\partial\eta}+z_\xi^2\frac{\partial^2}{\partial\eta^2}\right) \quad ,\text{and} \qquad (16)$$

$$+\xi_{rr}\frac{\partial}{\partial\xi}+\eta_{rr}\frac{\partial}{\partial\eta}$$

$$\frac{\partial^2}{\partial z^2}$$

$$= \frac{1}{J^2}\left(r_\eta^2 \frac{\partial^2}{\partial \xi^2} - 2 r_\xi r_\eta \frac{\partial^2}{\partial \xi \partial \eta} \right. $$
$$\left. + r_\xi^2 \frac{\partial^2}{\partial \eta^2} \right)$$
$$+ \xi_{zz} \frac{\partial}{\partial \xi} + \eta_{zz} \frac{\partial}{\partial \eta} \qquad (17)$$

The time differential can be also rewritten as

$$\frac{\partial}{\partial t} = \frac{\partial}{\partial t'} + \frac{1}{J}\left(z_\eta \frac{\partial}{\partial \xi} - z_\xi \frac{\partial}{\partial \eta} \right)\frac{\partial r}{\partial t'} $$
$$+ \frac{1}{J}\left(-r_\eta \frac{\partial}{\partial \xi} + r_\xi \frac{\partial}{\partial \eta} \right)\frac{\partial z}{\partial t'} \qquad (18)$$

Since t' is actually equal value to t, t' is replaced with t after here.

By substituting eqs. (14) – (18) to the governing equations, the transformed expression can be obtained. The energy transport equation, the vorticity transport equation, the stream function equation, and the energy balance equation are described as follows, respectively;

$$\rho\, C_p \left\{ \frac{\partial T}{\partial t} + \frac{1}{J}\left(z_\eta T_\xi - z_\xi T_\eta \right)\frac{\partial r}{\partial t} \right. $$
$$\left. + \frac{1}{J}\left(-r_\eta T_\xi + r_\xi T_\eta \right)\frac{\partial z}{\partial t} \right\}$$
$$- \rho\, C_p \frac{1}{r}\frac{1}{J}\left(\psi_\xi T_\eta - \psi_\eta T_\xi \right) \qquad , (19)$$
$$= \kappa \frac{1}{J^2}\left(\alpha T_{\xi\xi} - 2\beta T_{\xi\eta} + \gamma T_{\eta\eta} \right)$$
$$+ \kappa \frac{1}{r}\frac{1}{J}\left(z_\eta T_\xi - z_\xi T_\eta \right)$$

$$\frac{\partial \omega}{\partial t} + \frac{1}{J}\left(z_\eta \omega_\xi - z_\xi \omega_\eta \right)\frac{\partial r}{\partial t}$$
$$+ \frac{1}{J}\left(r_\eta \omega_\xi - r_\xi \omega_\eta \right)\frac{\partial z}{\partial t}$$
$$+ \frac{1}{r}\frac{1}{J^2}\left(-r_\eta \psi_\xi + r_\xi \psi_\eta \right)$$
$$\cdot \left(z_\eta \omega_\xi - z_\xi \omega_\eta \right)$$
$$- \frac{1}{r}\frac{1}{J^2}\left(z_\eta \psi_\xi - z_\xi \psi_\eta \right)$$
$$\cdot \left(-r_\eta \omega_\xi + r_\xi \omega_\eta \right)$$
$$- \frac{1}{r^2}\frac{1}{J}\omega\left(-r_\eta \psi_\xi + r_\xi \psi_\eta \right)$$
$$= \nu \frac{1}{J^2}\left(\alpha \omega_{\xi\xi} - 2\beta \omega_{\xi\eta} + \gamma \omega_{\eta\eta} \right)$$
$$+ \nu \frac{1}{r}\frac{1}{J}\left(z_\eta \omega_\xi - z_\xi \omega_\eta \right) - \nu \frac{1}{r^2}\omega$$
$$+ \frac{1}{J}B g\left(z_\eta T_\xi - z_\xi T_\eta \right) \qquad , (20)$$

$$-r J^2 \omega$$
$$= \alpha \psi_{\xi\xi} - 2\beta \psi_{\xi\eta} + \gamma \psi_{\eta\eta} \qquad , \text{and} \quad (21)$$
$$- \frac{J}{r}\left(z_\eta \psi_\xi - z_\xi \psi_\eta \right)$$

$$L_{SL}\, \rho \frac{\partial f}{\partial t}$$
$$= -\kappa_L \frac{1}{r_\xi}\frac{1}{J_L}\left(-\beta T_\xi + \gamma T_\eta \right)_L \qquad , (22)$$
$$+ \kappa_S \frac{1}{r_\xi}\frac{1}{J_S}\left(-\beta T_\xi + \gamma T_\eta \right)_S$$

where

$$\alpha = r_\eta^2 + z_\eta^2, \quad \beta = r_\xi r_\eta + z_\xi z_\eta,$$
$$\gamma = r_\xi^2 + z_\xi^2 \qquad (23)$$

In order to obtain eqs. (19) and (20), the following equations,

$$\xi_{rr} + \xi_{zz} = 0 \quad , \text{and} \qquad (23)$$

$$\eta_{rr} + \eta_{zz} = 0 \quad , \qquad (24)$$

are substituted. Equations (23) and (24) are the same as the equations that are used for grid generation. In order to generate a grid, the inverse expressions of eqs. (23) and (24),

$$\alpha r_{\xi\xi} - 2\beta r_{\xi\eta} + \gamma r_{\eta\eta} = 0 \quad , \text{and} \quad (25)$$

$$\alpha z_{\xi\xi} - 2\beta z_{\xi\eta} + \gamma z_{\eta\eta} = 0 \quad , \quad (26)$$

are used. These equations mean that the coordinates in the physical space are transformed to the coordinates in the calculation space as they are.

3. Calculation Results

Equations (25) and (26) are applied to an ampoule and a cartridge shown in Fig. 1 in order to generate a grid. These ampoule and cartridge are the present candidates for a flight experiment. The ampoule is based on the ampoule used in the past Japanese experiment under microgravity[2, 3], however, the present one is improved so that the convex interface shape can be obtained.

Since the ampoule is usually set in the cartridge as shown in Fig. 2, the whole cartridge is modeled. The grid in this model region, which is generated by using eqs. (12) and (13), is shown in Fig. 3. By using the grid, temperature, stream function, and vorticity distributions are calculated. The heating sequence is as follows; (i) melting back with heater speed of 5 mm/hr for 2 hours, (ii) stopping heater transfer for 1 hour, (iii) growing a crystal with heater speed of 1 mm/hr. It is assumed that a given temperature profile is formed on the surface and moves with the same speed as the heater transfer speed. The temperature profile is a combination of temperature gradients of 20 K/cm and 80 K/cm. The temperature is clipped so as to be a certain temperature range, 313 K to 1573 K. The end surface at the higher temperature side is assumed to be adiabatic. The end surface at the lower temperature side is well cooled and thus the temperature at this side is assumed to be equal to the temperature on the surface. The temperature profile and heating sequence is summarized and is shown in Fig. 4. The governing equations are transformed to the implicit difference equations and solved by the successive overrelaxation (SOR) method.

In order to investigate the difference between the interface shape under the microgravity and that on the earth, the gravity of both $1 \times 10^{-4}\ g$
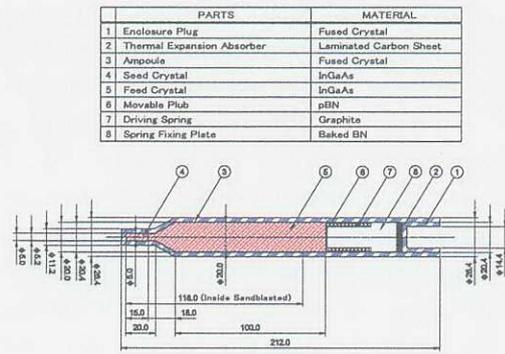

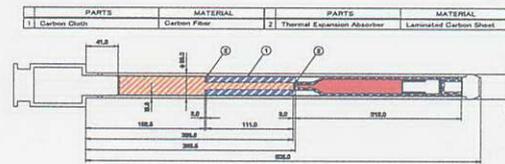Fig. 1　Schematic View of an Ampoule

Fig. 2　Schematic View of a Cartridge

Fig. 3　Generated Grids

and $1\ g$ is used. The used thermophysical properties are summarized in table 1. The typical results in cases of both the microgravity and the ground are shown in Fig. 5 and 6, respectively. The interface shape and its location in these cases are also traced and shown in Fig. 7 and 8, respectively.

From the calculation results, it is found that the interface shape is convex towards the melt in the backmelt phase and the shape changes from convex to W-shape in the growth phase. By comparing the shape under the microgravity with that on the ground, it is clarified that the shape on the ground is flatter than that under the microgravity due to thermal convection. The difference between the shapes in the backmelt phase and in the growth phase should be due to

the latent heat. In order to investigate the effect of the thermal convection on the interface shape, the shapes in a few gravity levels are compared and shown in Fig. 9. The interface shape is obtained at $t = 10800$ s. This means that the interface is at the initial interface location. Since the interface shape can be convex not only in space but also on the earth, results from ground-based experiments are useful for studying on the configuration of the flight ampoule and cartridge. The convex shape can be obtained by modeling the current candidates for the flight experiment, however, the convex region is not enough. Therefore, another improvement has to be investigated in future.

(a) Temperature

(b) Stream Function

(c) Vorticity

Fig. 5 Calculation Result ($1 \times 10^{-4} g$)

(a) Temperature

(b) Stream Function

(c) Vorticity

Fig. 6 Calculation Result ($1 g$)

(a) Backmelt Phase

(b) Crystal Growth Phase

Fig. 4 Heating Sequences

Table 1 Typical Thermophysical Properties

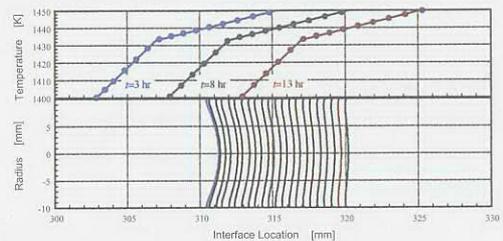| Material	Thermal Conductivity κ [W/(m·K)]	Density ρ [kg/m³]	Specific Heat C_p [J/(kg·K)]
Ta	60.2	16.36×10^3	1.54×10^2
WC-103	38.1 (1144 K) 40.7 (1386 K)	8.85×10^3	3.43×10^2
Cu	3.5×10^2	8.96×10^3	5.0×10^2
Fused Crystal	4.0	2.2×10^3	1.13×10^3
BN / pBN	7.0	2.0×10^3 (BN) 2.1×10^3 (pBN)	2.1×10^3
Carbon Cloth / Laminated Carbon Sheet	5.0	1.0×10^3	1.68×10^3
Graphite Spring	44.0	1.7×10^3	1.68×10^3
Arsenic Vapor (1 atm)	1.58×10^{-3}	1.45	1.0×10^3
Vacuum ($\sim 10^{-5}$ Torr)	9.2×10^{-11}	3.7×10^{-10}	1.01×10^3

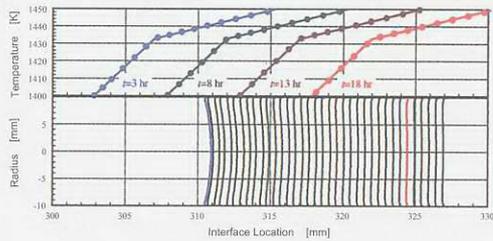(a) Backmelt Phase (Time Interval: 5 min.)

(b) Growth Phase (Time Interval: 30 min.)

Fig. 7 Interface Location ($1 \times 10^{-4} g$)
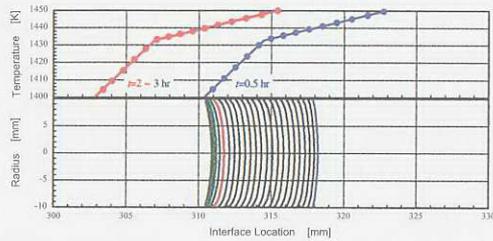
(a) Backmelt Phase (Time Interval: 5 min.)

(b) Growth Phase (Time Interval: 30 min.)

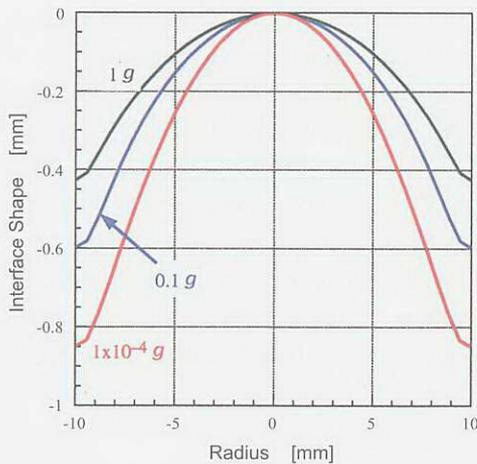Fig. 8   Interface Location (1 g)

Fig. 9   Comparison of Interface Shapes
($t = 10800$ s)

4. Experimental Result

In order to evaluate the reliability of the numerical analysis, calculation results must be compared with the experimental one. Since it is very difficult to obtain the result from the microgravity experiment, the experimental result on the earth is used as the reference data. The ampoule is schematically shown in Fig. 10. The photograph of the ampoule, which is nearly finished fabricating, is also shown in Fig. 11.

An InAs sample is used since this material has two elements which are also included in the target material, InGaAs, and since the interface shape is determined by only temperature. The experimental sequence is as follows; (i) the ampoule is slowly descended into a vertical gradient heating furnace and is set at the initial location, (ii) the ampoule and the furnace are maintained as they are to achieve the thermal equilibrium for more than 1 hour, and (iii) the furnace is transferred to make the sample directionally solidify. The obtained sample is shown in Fig. 12. Although the obtained sample is polycrystalline, the interface shape can be measured at a few locations. The measured shape is compared with the numerical one in the next section.
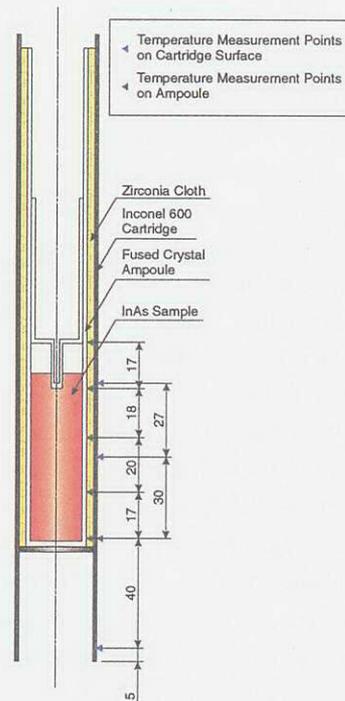

Fig. 10   Schematic View of an Ampoule for Ground Experiment

Fig. 11   Photograph of an Ampoule

—71—

Fig. 12　Sample Photograph

5. Discussion

In order to investigate the reliability of the calculation, another numerical calculation is carried out. In this calculation, another numerical model based on the experimental configuration is built. The grid generated by using this model is shown in Fig. 13. The grid region is based on the region where the temperature is measured. By using this grid, temperature, stream function, and vorticity are calculated. In this calculation, the temperature on the surface is given and both of end surfaces are assumed to be adiabatic. The temperature profile on the cartridge surface at the time of $t = 0$ is shown in Fig. 14. The time of $t = 0$ means the time just before starting solidification.

The obtained result at $t = 0$ and the interface location are shown in Fig. 15 and 16, respectively. The calculated interface shape is compared with the experimentally obtained one as shown in Fig. 17. In this figure, the z position of 19 mm means that the distance from the initial interface location is equal to 19 mm. The calculation result at the initial interface location well agrees with the experimental result. However, in the case of the calculation result at $z = 19$ mm, it seems that the interface shape does not so well agree with the experimentally measured shape.

In order to investigate the reason, the shape change along the longitudinal direction is computed. To obtain the quantitative expression of the shape, the shape is approximated by a function of $f(r) = a r^2$ and the proportional coefficient of the function, a, is used as the index of the quantitative expression. The change of the coefficient a is shown in Fig. 18. In Fig. 18, the closed circles represent the experimental data. As shown in Fig. 18, the trend of the experimental result is only about twice as steep as the trend of the calculation result. This difference can easily occur due to the little difference of the thermophysical parameters or the boundary conditions between the used value and the real value.

Another point of view on the reliability is a temperature profile. The calculation result is compared with the experimentally measured temperature as shown in Fig. 19. Fig. 19 shows that the calculated inner temperature profile well agrees with the measured temperature. The maximum error is about 3 percent. This indicates that the temperature distribution is precisely computed in general.

The tendency of the interface shape change has relatively larger error as compared with the error of the temperature profile. This suggests that the thermophysical parameters required for the temperature calculation, that is, thermal conductivity, density, and specific heat, are not so different from the proper values. On the other hand, the latent heat is used for the only calculation of the interface shape and location. This also suggests that the latent heat might have the relatively large error.

−72−

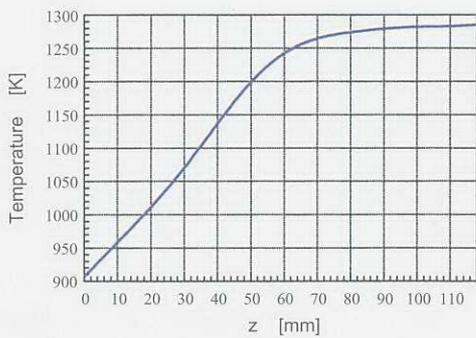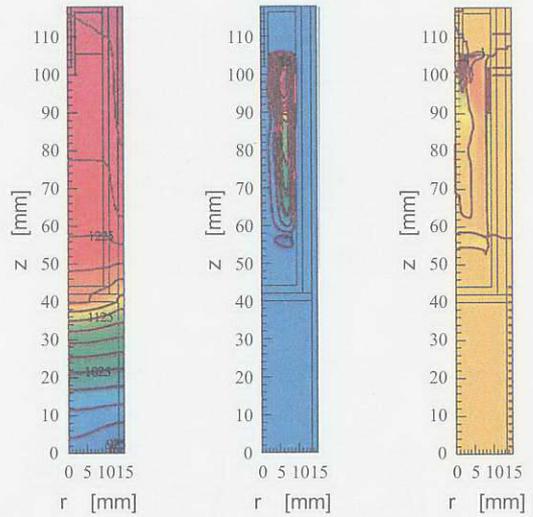Fig. 13   Generated Grid

Fig. 14   Temperature Profile

(a) Temperature (b) Stream Function (c) Vorticity

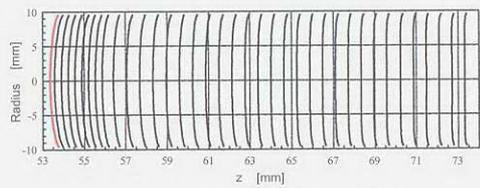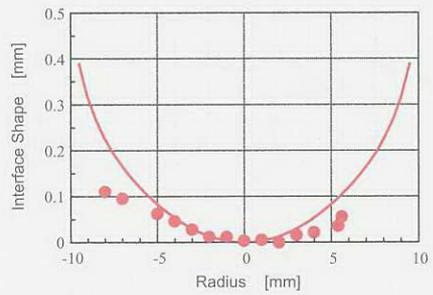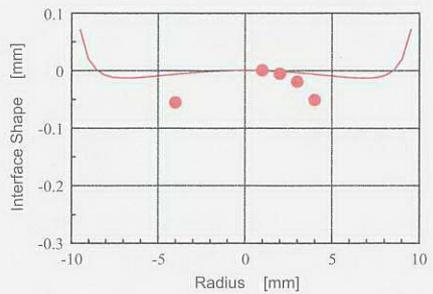Fig. 15   Calculation Result

Fig. 16   Interface Location

(a) Initial Location

(b) $z = 19$ mm

Fig. 17   Comparison between Calculation and
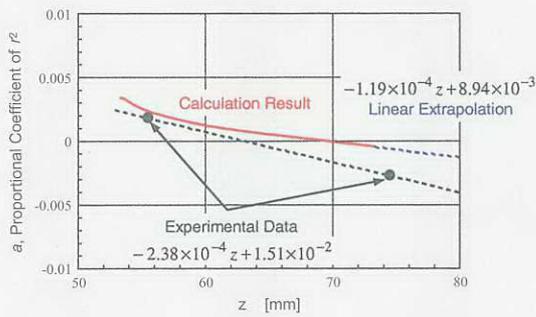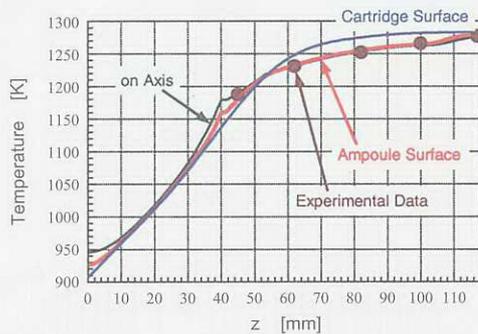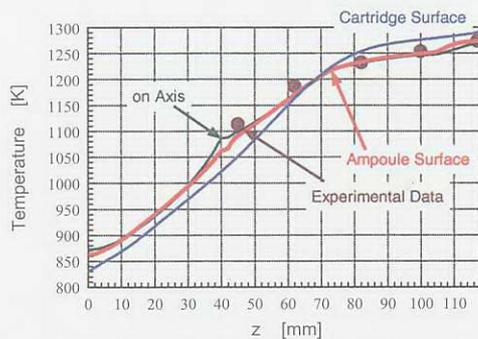Experimental Results

Fig. 18 Trend of Interface Shape Change

(a) Initial Interface Location

(b) z = 19 mm

Fig. 19 Calculated Temperature Profile

6. Conclusions

In order to investigate the way to obtain the convex interface shape, the nonsteady state numerical calculation is carried out. The calculation code is originally developed and is based on the BFC method in cylindrical coordinates. From the computational result, it is found that the convex shape can be obtained in the limited region in the case of the candidates for the flight ampoule and the flight cartridge.

In order to investigate the reliability of the calculation, the calculation result is compared with the ground-based experimental result. It is

found that the computed shape at the initial location well agrees with the experimental one. Although the divergence between the numerically obtained and experimentally obtained shapes gradually increased with the longitudinal direction, the trend slope of the experiment is only twice as steep as the trend slope of the calculation. It is also found that the calculated internal temperature profile well agrees with the measured temperature. By considering those results, the divergence might be caused by the value error of the latent heat.

The interface shape is the common problem in order to grow a single crystal. The numerical analysis, such as the calculation in this paper, will be effective method of solving the problem. And the experimental result obtained under the microgravity, too. Namely, there is the possibility that the results of the research related to the microgravity experiment can be applied to the research on the earth. This is one of the most important points of view in the present microgravity experiment.

References

[1] J. M. Bly, M. L. Kaforey, D. H. Matthiesen and A. Chait: *Proc. of the 1996 10th American Conf. on Cryst. Growth and the 9th Int. Conf. on Vapor Growth and Epitaxy, Vail, 1996,* J. Cryst. Growth, **174** (1997) Suppl. 1-4, pp. 220-225.

[2] S. Adachi, M. Miyuki, K. Takahashi and H. Sakai: *Proc. of Symp. on SFU Experiments for Industries, Tokyo, 1996* (Institute for Unmanned Space Experiment Free Flyer, 1996).

[3] S. Adachi, K. Takahashi and Y Ikegami: Abstr. (123rd TMS Annual Meet. and Exhibition 1994); The Mineral, Metals & Materials Society, p.22.

4) J. F. Thompson, F. C. Thames and C. W. Mastin: J. Comp. Phys. **15** (1974) 299.

5) K. Fujii: *Numerical Methods for Computational Fluid Dynamics* (Tokyo Univ., Tokyo, 1994) 2nd ed., Chap. 7 [in Japanese].

6) H. Takami and T. Kawamura: *Numerical Solution of Partial Differential Equations by the Finite Difference Method* (Tokyo Univ., Tokyo, 1994) 2nd ed., Chap. 6 [in Japanese].

7) M. Saitou: Inst. Electron. Mater. Tech. Note **7** (1989) No. 2, 15 [in Japanese].